IEEE Access
Multidisciplinary | Rapid Review | Open Access Journal

Received June 2, 2021, accepted June 14, 2021, date of publication June 17, 2021, date of current version June 28, 2021.

Digital Object Identifier 10.1109/ACCESS.2021.3090078

A Single Image Dehazing Technique Using the Dual Transmission Maps Strategy and Gradient-Domain Guided Image Filtering

SYED MUHAMMAD EHSAN[1], MUHAMMAD IMRAN[2,3], ANAYAT ULLAH[1,3], AND ERSIN ELBASI[4]

[1]Department of Electronic Engineering, FICT, Balochistan University of Information Technology, Engineering, and Management Sciences (BUITMES), Quetta 87300, Pakistan
[2]Department of Electrical Engineering, FICT, Balochistan University of Information Technology, Engineering, and Management Sciences (BUITMES), Quetta 87300, Pakistan
[3]Control, Automotive, and Robotics Laboratory, National Center of Robotics and Automation, Rawalpindi 46000, Pakistan
[4]College of Engineering and Technology, American University of the Middle East, Egaila 15453, Kuwait

Corresponding author: Muhammad Imran (engr.imran@buitms.edu.pk and mi14@my.fsu.edu)

This work was supported by the Control Automotive and Robotics Laboratory (CARL), National Center of Robotics and Automation (NCRA), Balochistan University of Information Technology, Engineering, and Management Sciences (BUITMES), with the collaboration of Higher Education Commission (HEC) of Pakistan.

ABSTRACT In this paper, a single image dehazing technique using dual transmission maps strategy and gradient-domain guided image filtering is presented. A new strategy is adopted to compute the dual transmission maps using the dark channel and atmospheric light. Further, the transmission maps are refined to remove any remaining ill effects using the gradient-domain-guided filter. Finally, using the dark channel, atmospheric light, and refined transmission map, the haze-free image is obtained. The dual transmission maps strategy not only removes halo artifacts and reduces the saturation but also ensures the natural appearance in the recovered images. Furthermore, the proposed scheme is evaluated using a wide range of images and compared with state-of-the-art schemes. The comparison shows the superiority of the proposed technique in terms of recovering haze-free images.

INDEX TERMS Image de-hazing, transmission map, gradient-domain guided image filter.

I. INTRODUCTION

Adverse weather, when taken outdoor images, could often decline the quality of images significantly. The degradation in the perceptual quality is due to the particles present in the atmosphere like fog, dust, mist, and haze [1]. The presence of haze in the atmosphere obscures the clarity of the scene. The reflection of suspended particles like fog, haze, and mist in the atmosphere causes scattering and attenuation. The scattering and attenuation subsequently reduce the direct transmission from the scene to the camera and add another layer of the surrounding scattered light, known as ambient light [2], [3]. The attenuated direct transmission causes the observed image to suffer from low visibility, loss of contrast, and faded color, as shown in Fig. 1.

As a result, computer vision applications, such as object detection, road sign or traffic signal recognition, etcetera, find it difficult to extract and utilize the complete information from the images. To remove the effect of weather and make images more comprehensible, image-dehazing is proposed as a prominent solution [4]–[6]. The task of image dehazing is to remove the effects of haze, which, in turn, sometimes causes essential information to be removed; therefore, in image dehazing, one of the challenges is to remove the ill effects of weather while maintaining the general details.

FIGURE 1. Hazy images.

The associate editor coordinating the review of this manuscript and approving it for publication was Khursheed Aurangzeb.

This work is licensed under a Creative Commons Attribution 4.0 License. For more information, see https://creativecommons.org/licenses/by/4.0/

In recent years, the computer vision field has found applications almost everywhere: remote sensing [7], smart vehicles [8], objection identification [9], outdoor monitoring [10], supervision [11], etcetera. However, in these computer vision applications, input images need to be perceptually clear, which sometimes not possible due to the heterogeneous environment. So, it is necessary to restore haze-free images rapidly and efficiently for computer vision applications. Due to the uncertainty of weather itself and more unknown variables dehazing single images has always been a difficult task [12], [13]. Dehazing methods are mainly divided into two types: enhancement-based [12]–[14] and restoration-based dehazing methods. The former approach, somehow, improves the quality of resultant images but loses details, especially near edges. The latter approach - such as color attenuation prior [15] and dark channel prior [16], [17] - on the other hand, obtain quality haze-free images and retain the crucial information by maximizing the local contrast of the input hazy image and enhances the visibility of degraded images.

Recently, a significant amount of research has been carried out on single image dehazing algorithms, which improves the efficiency, computational time, and quality of degraded images [16]–[18]. The algorithms improve several characteristics of hazy images, such as visibility, contrast, and produce the natural color of output images due to better assumptions and priors. In [18], a dehazing method is proposed, which removes the haze from a single image using a dark channel prior. The method is widely used in many image dehazing algorithms. The proposed algorithm is based on the statistical approach of the dark channel. The algorithm recovers an image with high quality and maintaining the general details of the original image using soft matting - a very complex and time-consuming algorithm - for the refinement of the transmission map. The proposed method, however, causes halo-artifacts and color alteration, and failed when the input image contains a large sky region. The method proposed in [19] is an efficient method for image dehazing, and it uses the L_1 norm based optimization method to estimate the unknown scene transmission. The suggested method can recover a good quality haze-free image with fine color and rich details, but this method utilizes a very complex refinement strategy. The fusion-based method [20] is another method that can remove haze from a single image efficiently by computing three weight maps in a per-pixel fashion. The halo artifacts introduced by these weight map is minimized by multi-scale fashion using a Laplacian pyramid. The proposed algorithm gives very comparative results as compared to the previous methods. The drawback of this method, however, is high computational time that, in turn, makes it unsuitable for real-time applications. The method in [21] suggested a unique and hybrid approach of combining dark channel prior and bright channel before restoring a haze-free image from the hazy image. The method overcomes computational time; a guided filter is used for transmission map refinement. The algorithm proposed in [22] is based on a globally guided image filter, which improves the color contrast of the hazy image and preserves edge information in the resultant dehazed image, but the method introduces some halo artifacts in the dehazed image. Most of the techniques, discussed so far, experience hindrances like computational complexity and fail to achieve good results for images containing large sky regions. To solve this problem of sky failure, a very effective and efficient method has been proposed in [23]. The method reduced overexposure problems and color alteration in the sky and bright regions. The method proposed in [24] is a very fast and efficient dehazing single image algorithm that uses a dark channel and morphological reconstruction processes to refine the transmission map and avoid computational complexity. The proposed method recovers high-quality haze-free images with enriching details. The technique presented in [25] uses a dark channel prior to estimate different atmospheric light values for the sky and non-sky regions. The proposed method shows good results of images containing a large sky region. Dehazing techniques based on variational models [26]–[29] also exists in the literature. Variational models [26] employ an iterative strategy to optimize a function to find either the best possible minima or maxima using the calculus of variations. Due to their iterative nature, they take comparatively longer time to estimate the best transmission map and, hence, are unsuitable for real-time applications.

In addition to conventional computer vision approaches to solving the dehazing problem, numerous methods based on machine and deep learning have been proposed [30]–[33]. For instance, the methods [30] and [31] dehaze a hazy image using multilayer perceptrons, and the method [31] dehazes images using a trainable end-to-end multi-scale convolutional neural network. Similarly, the approach presented in [32] using NIN-DehazeNet combining Network-in-Network with MSCNN (Single Image Dehazing via Multi-Scale Convolutional Neural Networks) to estimate transmission map. Neural network-based dehazing methods give good results, but, like other neural-network-based techniques, they need large datasets and high computational resources. These requirements make them unsuitable for real-life applications.

Though the existing schemes give good results in terms of haze removal, they still have some shortcomings, such as complex algorithms, color-distortions in the recovered image, and high computational time. Therefore, in the paper, we have proposed a scheme that is not only simple but provides good results. There are many minor contributions of the presented paper, but the major ones are three: (i). the computation of dual transmission maps, (ii). the fusion of dual transmission maps, and (iii). the refinement of the fused transmission map. The details of these contributions are mentioned in the Secs. II and III.

The rest of the paper is organized as follows: in Sec. II, we discuss the mathematical background required to understand the proposed algorithm, Sec. III is dedicated to the proposed scheme, while Sec. IV and Sec. V are reserved for experimental results and conclusion, respectively.

II. BACKGROUND

The proposed technique utilizes three parameters: atmospheric dispersion model, dark channel prior, and transmission map; therefore, in this section, these parameters along with other information are discussed in detail.

A. ATMOSPHERIC DISPERSION MODEL

The atmospheric dispersion model is a physical model used for the formation of haze [1]. The mathematical model for hazy image formation is described in Eq. (1).

$$f(x, y, c) = g(x, y, c)t(x, y) + A(1 - t(x, y)) \quad x, y \in \mathbb{R}^{(X,Y)} \tag{1}$$

where $f(x, y, c)$ is the captured hazy image, A is the ambient light value, $g(x, y, c)$ is the scene radiance, and $t(x, y)$ is the scene transmission medium – describing the portion of the light that is not scattered and reaches the camera. Finally, $(x, y) \in \mathbb{R}^{(X,Y)}$ denote the coordinates of pixels and $c \in \mathbb{R}^3$ represents the number of channels.

The target of a haze removal algorithm is to recover g, A, and t from f. In Eq. (1), the first term; that is, $g(x, y, c)t(x, y)$, represents the direct attenuation [1], [2], which denotes the portion of light, that after attenuating through the medium, reaches the camera. The second term; that is, $A(1-t(x, y))$, denotes the atmospheric scattering light, which causes the distortion, contrast reduction, and color shift in a scene.

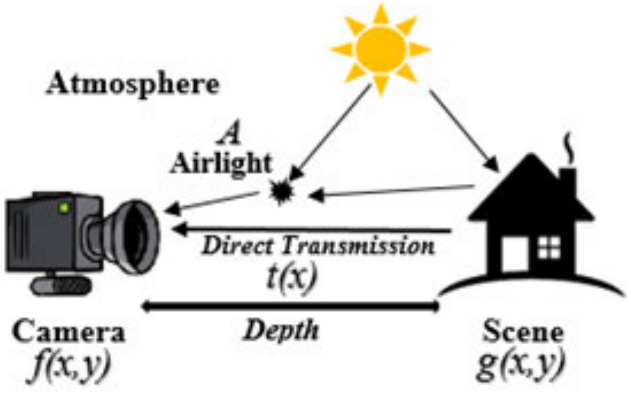

FIGURE 2. Atmospheric dispersion model.

Fig. 2, which is shown above, depicts the atmospheric dispersion model. The ambient light value (A), some authors refer it as airlight other calls it atmospheric light, represents tiny particles scattering in the atmosphere and mix with the sunlight, and, as a result, create contrast reduction and distortion in the scene. The direct transmission $t(x, y)$ denotes the amount of light that reaches the camera without distortion, and the depth shows the distance between the camera and the scene to be captured.

B. DARK CHANNEL PRIOR (DCP)

For any hazy image $f(x, y, c)$, the dark channel [18] is computed as follows:

$$g^{dark}(x, y) = \min_{p \in \Omega(m,n)} \left(\min_{c \in \{r,g,b\}} f(x, y, c) \right), \tag{2}$$

where $\Omega(m, n)$ represents the local patch, which is centered at (m, n). The resultant dark channel $g^{dark}(x, y)$ is a haze-free image and contains zeros where the region is non-bright and non-zeros values otherwise, as shown in Fig. 3. For a detailed explanation of the dark channel prior, readers can refer to [18].

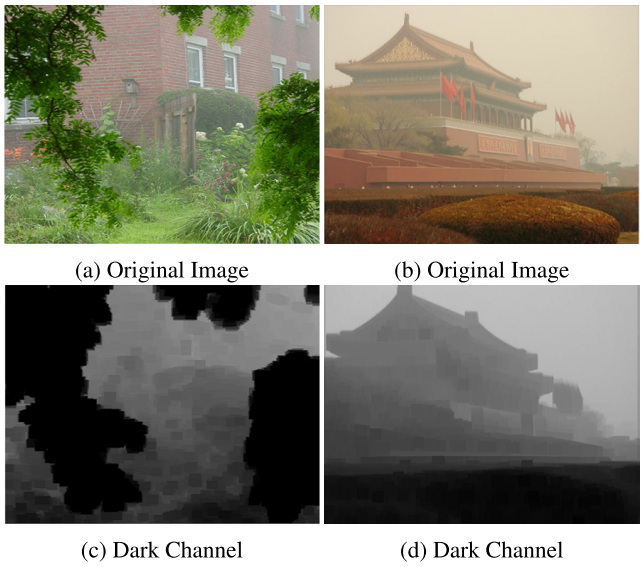

FIGURE 3. Images and their dark channels.

C. ATMOSPHERIC LIGHT ESTIMATION

The reflection of suspended particles like fog, haze, and mist in the atmosphere causes scattering and attenuation. The scattering and attenuation reduce the direct transmission from the scene to the camera and adds another layer of the surrounding scattered light, known as atmospheric light. The atmospheric light reduces the quality of input images; therefore, a suitable method is required to estimate the atmospheric light. There are several methods [18], [20], [23] for the estimation of atmospheric light. In the proposed method, the atmospheric light [18] for each color channel is estimated using the steps described in Algorithm 1.

As a result, the atmospheric light would be a three dimensional vector; that is, $A \in \mathbb{R}^{1\times3}$, where each value representing the atmospheric light of each channel.

D. TRANSMISSION MAP ESTIMATION

The transmission map $t(x, y)$ denotes the portion of the light that reaches the camera after reflecting from the scene. As a result, it contains the depth information of the haze in the degraded image. The transmission map estimation plays

Algorithm 1 Atmospheric Light Estimation

Input: $f(x, y, c) \in \mathbb{R}^{X \times Y \times C}$: Hazy Source Image, $g^{dark}(x, y) \in \mathbb{R}^{X \times Y}$: Dark Channel of Hazy Image.
Output: $A \in \mathbb{R}^{1 \times C}$: Atmospheric Light Estimation

1 $[val, ind] = \max_{i=0}^{q} \left(g^{dark}(x, y)\right)$
/* find the q number of bright pixels and their locations from the dark channel g^{dark} */
2 **for** $i \leftarrow 1$ **to** C **do**
3 $g(1, i) = f(ind, i)$
/* finding the q pixels of each channel of f located at locations ind */
4 **end**
5 $A = \frac{g(1,C)}{q}$; // Computing the mean of $g(1, C)$

Algorithm 2 Transmission Map Estimation

Input: $f(x, y, c) \in \mathbb{R}^{X \times Y \times C}$: Hazy Source Image, $A \in \mathbb{R}^{1 \times C}$: Atmospheric Light of each Channel.
Output: $t(x, y) \in \mathbb{R}^{X \times Y}$: Transmission Map Estimation

1 **for** $i \leftarrow 1$ **to** C **do**
2 $J(x, y, i) = \frac{f(x,y,i)}{A(1,i)}$
/* dividing all the pixels of the original image with the corresponding airlight estimation */
3 **end**
4 Dark channel computation $f^{dark}(x, y)$ using Eq. (2)
5 $t(x, y) \leftarrow 1 - \omega * f^{dark}(x, y)$; // estimation map is computed

a crucial role in image dehazing because, without the information of the depth, it is almost impossible to de-haze an image.

The transmission map is computed as described in the Algorithm 2.

On a normal clear day, some tiny particles are present in the atmosphere; therefore, a constant parameter: $\omega \in [0, 1]$, is introduced in Step 5 of Algorithm 2 to keep the small amount of haze for the practical situation [18].

E. REFINEMENT OF THE TRANSMISSION MAP

The transmission map estimated using Algorithm 2 contains some halo artifacts near the edges of hazy images. The reason is that the transmission map is not always constant in the patch. Many methods were proposed to refine the rough transmission map such as soft matting [18], guided filter [22], and some other refinement methods were presented in [24] and [30]. However, in the proposed scheme, we have employed gradient-domain guided image filtering [34] to refine the transmission map. The involvement of the gradient-domain guided filter improves the computational time, which is required in image dehazing algorithms to make them suitable for practical use [19], [20].

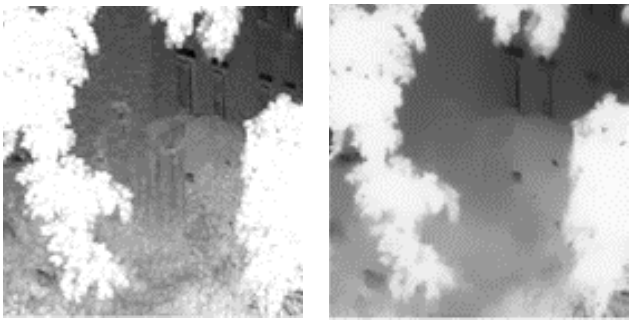

(a) Rough Estimation Map (b) Refined Estimation Map

FIGURE 4. Estimation maps.

The filter not only reduces the computational time but brings natural appearance in the transmission map as compared to the existing methods, also evident from Fig. 4.

III. PROPOSED METHOD

In image dehazing, the size of a window plays an important role [1], [4]. For instance, a smaller window size, such as 3×3, reduces halo artifacts effectively; however, it increases the computational time and makes the restored images over-saturated. Furthermore, the smaller windows are sensitive to noise. On the other hand, a comparatively larger window size, such as 15×15 or more, reduces the saturation and helps in estimating the accurate atmospheric light, but it produces halo artifacts, especially near edges [23], [24]. Therefore, selecting a suitable filter size is of paramount importance. In the proposed method, it is found out that using both the sizes: small and large, eliminates the phenomenon of color saturation, halo artifacts, and enriches the details of the restored image. The detailed procedure of the proposed scheme is shown in the diagram of Fig. 5.

Given a hazy image $f(x, y, c) \in \mathbb{R}^{X \times Y \times C}$, first, the dark channel prior $g^{dark}(x, y)$ is computed using Eq. 2. Next, the atmospheric light estimate: $A \in [0, 1]$, is calculated using Algorithm 1. The parameter A contains three values, which will show how much each channel of the hazy image has suffered due to the atmosphere. The parameter (A) is then used to estimate the transmission map. To avoid any halo artifacts and over-saturation in the restored images, dual transmission maps are estimated: one with a smaller window and the other with a larger window size. In this research, we found out that, using sizes of 3×3 and 15×15 for smaller and larger windows, respectively, give satisfactory results as shown in Sec. IV. Later, both the transmission maps are combined as follows:

$$t(x, y) = \alpha t_1(x, y) + (1 - \alpha) t_2(x, y), \tag{3}$$

where $\alpha \in (0, 1)$ is used as a regularization parameter to control the contribution of each transmission map in the

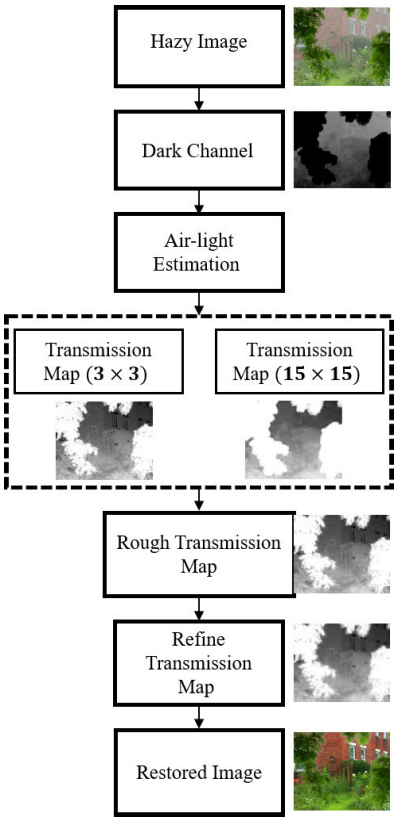

FIGURE 5. Atmospheric dispersion model.

final image. To select a suitable value for α, we performed a number of experiments. Our experiments revealed that the larger value of α introduces over-saturation in the resultant image and makes it perceptually unnatural. The smaller values; that is, less than 0.5, on the other hand, cause haze to remain in the output image. The optimal value for α that we found is 0.85, which gives good results in terms of haze removal and keeps the natural appearance intact. Therefore, in the proposed scheme, the value $\alpha = 0.85$ is used.

Though the dual transmission map strategy reduces halo artifacts and over-saturation, the estimated transmission map $t(x, y)$ still contains some halo artifacts. To remove them and to estimate the refined transmission map $\tilde{t}(x, y)$, gradient domain guided image filtering [34] is used. To apply the filter, the gray-scale version of the hazy image is used as a reference image. Finally, the restored (haze-free) image is obtained using the following equation.

$$g(x, y, c) = \frac{f(x, y, c) - A}{\max\left(\tilde{t}(x, y), t_o\right)} + A \tag{4}$$

The value $t_o = 0.1$ is introduced in the above equation to avoid the division by 0 and to bring the natural appearance in the restored image.

IV. EXPERIMENTAL RESULT

To validate the performance of the proposed scheme, a number of experiments were performed. The images [35] and [36], chosen for experimentation, have a wide range of varieties. Furthermore, the presented scheme is analyzed subjectively and objectively, and compared with some state-of-the-art techniques [15], [18], [24], and [39]. In the subsequent subsections, the performance of the proposed scheme and its comparison with other techniques are discussed in detail.

A. SUBJECTIVE COMPARISON

To prove the quality of our scheme, the first image, shown in Fig. 6a, is chosen. The opted figure is very diverse; it not only contains structural variation, but also contains a wide range of colors. From Fig. 6, it is visible that all the schemes were successful in restoring the haze-free image. However, upon zooming the pictures, it is revealed that some of them are blurry, while others are over-saturated as shown in Fig. 6. For instance, the results of the technique [18] contain halo artifacts around leaves and the overall image look dim; the method [24], shown in Fig. 6d, recovers good quality images and removes the haze very well, but images look blur and over-saturated; the result of [15], shown in Fig. 6c, contains halo artifacts near edges, the whole image is darker, and the result looks unnatural.

On the contrary, the proposed scheme not only removes the haze but brings the natural appearance with brightness in the

FIGURE 6. Comparison with state-of-the-art schemes.

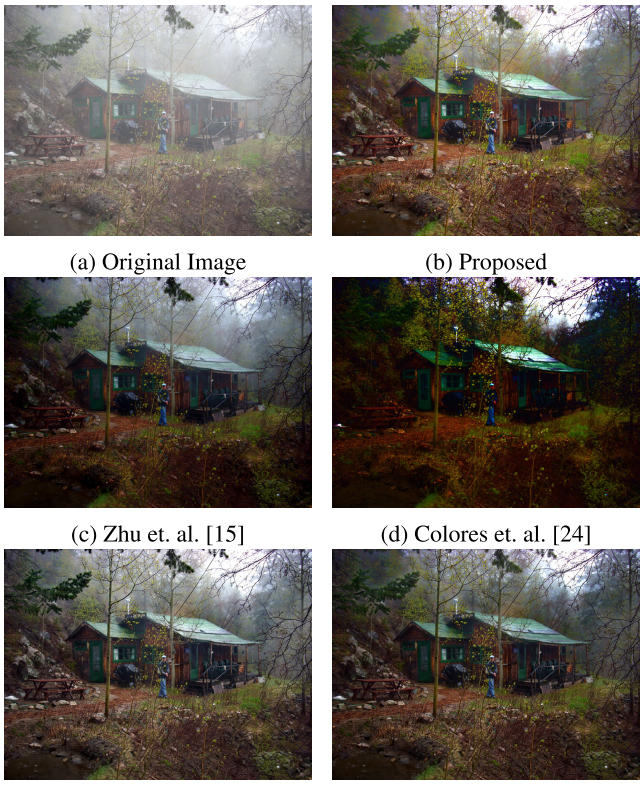

FIGURE 7. Comparison with state-of-the-art schemes.

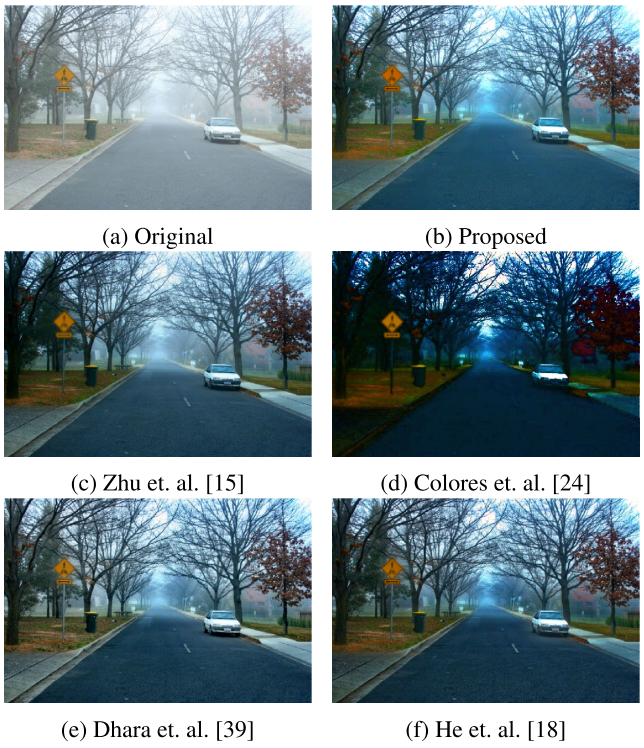

FIGURE 8. Comparison with state-of-the-art schemes.

restored image while maintaining the details of the original image at the same time.

To further strengthen the validation of the better performance of the proposed scheme as compared to the existing techniques, a detailed comparison is presented in Fig. 7. The techniques [15], [18], and [39] could somehow remove the haze, but the sky region still has a significant amount of haze. The technique [24], on the other hand, successfully removed the haze; however, the resultant image is over-saturated and, therefore, appears dark. Whereas, the proposed technique not only removed the haze but ensured the perceptual quality in terms of brightness, and, as a result, the resultant images look natural with all the details.

The comparison of the proposed scheme with other contemporary schemes for another outdoor image 8a is shown in Fig. 8. The proposed scheme outperforms [24] in terms of qualitative performance. However, the improvement in comparison to [15], [18], and [39] is very subtle; for instance, all the images look similar, but upon zooming, it appears the proposed scheme's image is crisper and retains the edge information when removing haze; while other techniques loss this crispness.

The proposed scheme is tested for a number of images, and it is space-consuming to discuss each image one by one. Therefore the results of the presented scheme along with original images are shown in Fig. 9. It is evident from Fig. 9 that the proposed scheme is successful in removing the haze from a range of images of different textures and varieties and recovered haze-free images.

TABLE 1. Evaluation and comparison in terms of PSNR.

Images	Proposed	Zhu et. al. [15]	He et. al. [18]	Colores et. al. [24]	Dhara et. al. [39]
1	17.2678	15.7072	15.2408	10.5534	**19.6282**
2	**10.9777**	8.7919	8.4679	7.9470	10.6896
3	**17.2268**	14.2792	12.4969	11.4767	16.3664
4	**11.8231**	9.6010	10.2931	6.6657	11.0233
5	**10.7390**	8.6277	9.3269	7.1793	9.8030
6	**14.9563**	11.9693	14.1965	9.4888	13.3835
7	**13.9790**	9.7382	10.2164	5.8558	10.8255
8	**14.9208**	12.0485	13.8498	8.9657	12.9245
9	**13.8451**	11.7174	11.4434	9.1193	12.7679
10	**12.8870**	9.9603	9.8219	6.9637	12.1355
11	**10.5121**	8.5723	10.3463	6.7677	9.9013
12	14.4104	12.1845	**14.8050**	9.5647	13.1990

B. OBJECTIVE COMPARISON

In addition to subjective analysis and qualitative comparison with other schemes, the proposed scheme is evaluated and

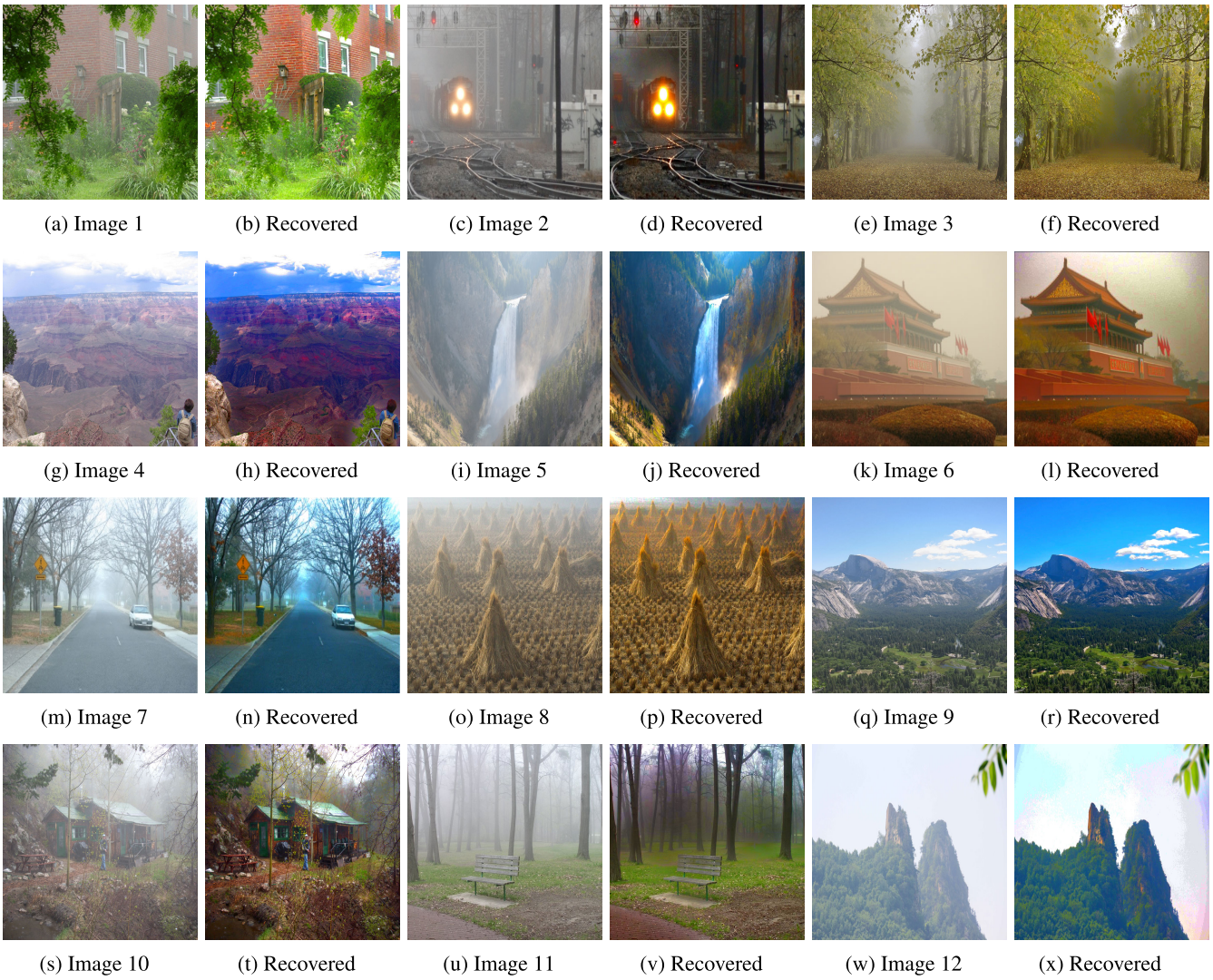

(a) Image 1 (b) Recovered (c) Image 2 (d) Recovered (e) Image 3 (f) Recovered

(g) Image 4 (h) Recovered (i) Image 5 (j) Recovered (k) Image 6 (l) Recovered

(m) Image 7 (n) Recovered (o) Image 8 (p) Recovered (q) Image 9 (r) Recovered

(s) Image 10 (t) Recovered (u) Image 11 (v) Recovered (w) Image 12 (x) Recovered

FIGURE 9. Original and recovered images.

compared with the latest techniques objectively as well. For objective analysis and comparison, peak signal-to-noise ratio (PSNR) [24] is used. Before proceeding further, the PSNR is discussed briefly in the forthcoming subsection.

1) PEAK SIGNAL-TO-NOISE RATIO (PSNR)

The PSNR calculates the peak signal-to-noise ratio between two images in decibels. The higher value of PSNR indicates better performance of a scheme to recover the haze-free images. Given a hazy image $f(x, y, c)$ and recovered haze-free image $g(x, y, c)$, the PSNR is computed as follows:

$$PSNR = 10 \log_{10} \left(\frac{I_{max}^2}{MSE} \right), \tag{5}$$

where I_{max}^2 and MSE represent, respectively, the maximum possible value in the image $g(x, y, c)$ and the mean squared error between $g(x, y, c)$ and $f(x, y, c)$. The MSE can be computed using (6).

$$MSE = \frac{1}{m \times n \times c} \sum_{c=1}^{C} \sum_{x=1}^{X} \sum_{y=1}^{Y} (f(x, y, c) - g(x, y, c))^2 \tag{6}$$

TABLE 2. Comparison in terms of computational time.

Methods	Computational Time (in seconds)
Proposed Scheme	**2.546787**
Zhu et. al. [15]	2.849918
He et. al. [18]	3.362177
Colores et. al. [24]	3.508036
Dhara et. al. [39]	3.603959

Finally, the PSNR values of the proposed scheme and other techniques are presented in Table 1.

It can be seen that the proposed scheme performed better than other state-of-the-art schemes.

To carry out the experiments, we used MATLAB (2018 version) software on a computer with specifications: 2GB RAM, Windows 8 operating system, and Intel core i3 processor. Furthermore, the computational time of our scheme and that of others is presented in Table 2.

It is visible that our scheme outperforms the contemporary techniques in terms of processing speed as well.

V. CONCLUSION

In this paper, we introduce a very simple, effective, and time-efficient method is proposed for image dehazing. To achieve haze-free images, a dark channel is used and dual transmission maps are estimated using different window sizes. The proposed method has been tested on different images and compared with state-of-the-art methods. The experimental result shows that the proposed method can effectively recover the haze-free image with true color and reduces the computational time as well. This method for image dehazing offers a fast high-performance dehazing algorithm that is suitable for high-resolution images and computer vision applications. However, the proposed technique struggles to remove haze from those hazy images, which are taken at nighttime. In the future, we would like to propose a solution that can remove haze regardless the images are taken in daytime or nighttime.

REFERENCES

[1] Y. Xu, J. Wen, L. Fei, and Z. Zhang, "Review of video and image defogging algorithms and related studies on image restoration and enhancement," *IEEE Access*, vol. 4, pp. 165–188, 2016, doi: 10.1109/ACCESS.2015.2511558.

[2] S. Lee, S. Yun, J.-H. Nam, C. S. Won, and S.-W. Jung, "A review on dark channel prior based image dehazing algorithms," *EURASIP J. Image Video Process.*, vol. 2016, no. 1, pp. 5–23, Dec. 2016, doi: 10.1186/s13640-016-0104-y.

[3] W. Ren, L. Ma, J. Zhang, J. Pan, X. Cao, W. Liu, and M.-H. Yang, "Gated fusion network for single image dehazing," in *Proc. IEEE/CVF Conf. Comput. Vis. Pattern Recognit.*, Jun. 2018, pp. 3253–3261, doi: 10.1109/CVPR.2018.00343.

[4] W. Mei and X. Li, "Single image dehazing using dark channel fusion and haze density weight," in *Proc. IEEE 9th Int. Conf. Electron. Inf. Emergency Commun. (ICEIEC)*, Jul. 2019, pp. 579–585, doi: 10.1109/ICEIEC.2019.8784493.

[5] W. Wang and X. Yuan, "Recent advances in image dehazing," *IEEE/CAA J. Automatica Sinica*, vol. 4, no. 3, pp. 410–436, Jul. 2017, doi: 10.1109/JAS.2017.7510532.

[6] S. Salazar-Colores, J.-M. Ramos-Arreguín, J.-C. Pedraza-Ortega, and J. Rodríguez-Reséndiz, "Efficient single image dehazing by modifying the dark channel prior," *EURASIP J. Image Video Process.*, vol. 2019, no. 1, pp. 1–8, Dec. 2019, doi: 10.1186/s13640-019-0447-2.

[7] Y. Xu, B. Du, L. Zhang, D. Cerra, M. Pato, E. Carmona, S. Prasad, N. Yokoya, R. Hänsch, and B. L. Saux, "Advanced multi-sensor optical remote sensing for urban land use and land cover classification: Outcome of the 2018 IEEE GRSS data fusion contest," *IEEE J. Sel. Topics Appl. Earth Observ. Remote Sens.*, vol. 12, no. 6, pp. 1709–1724, Jun. 2019, doi: 10.1109/JSTARS.2019.2911113.

[8] R. Srinivasan, A. Sharmili, S. Saravanan, and D. Jayaprakash, "Smart vehicles with everything," in *Proc. 2nd Int. Conf. Contemp. Comput. Informat. (IC3I)*, Dec. 2016, pp. 400–403, doi: 10.1109/IC3I.2016.7917997.

[9] C. Tang, Y. Feng, X. Yang, C. Zheng, and Y. Zhou, "The object detection based on deep learning," in *Proc. 4th Int. Conf. Inf. Sci. Control Eng. (ICISCE)*, Jul. 2017, pp. 723–728, doi: 10.1109/ICISCE.2017.156.

[10] Y.-L. He, S.-Q. Geng, X.-H. Peng, L.-G. Hou, X.-K. Gao, and J.-H. Wang, "Design of outdoor air quality monitoring system based on ZigBee wireless sensor network," in *Proc. 13th IEEE Int. Conf. Solid-State Integr. Circuit Technol. (ICSICT)*, Oct. 2016, pp. 368–370, doi: 10.1109/ICSICT.2016.7998923.

[11] A. Vega, F. Santamaria, and E. Rivas, "Supervision, monitoring and control of home appliances through power line communication," in *Proc. IEEE PES Transmiss. Distrib. Conf. Exhib. Latin Amer. (T&D-LA)*, Sep. 2018, pp. 1–5, doi: 10.1109/TDC-LA.2018.8511636.

[12] L. T. Thanh, D. N. H. Thanh, N. M. Hue, and V. B. S. Prasath, "Single image dehazing based on adaptive histogram equalization and linearization of gamma correction," in *Proc. 25th Asia–Pacific Conf. Commun. (APCC)*, Nov. 2019, pp. 36–40, doi: 10.1109/APCC47188.2019.9026457.

[13] J. He, C. Zhang, R. Yang, and K. Zhu, "Convex optimization for fast image dehazing," in *Proc. IEEE Int. Conf. Image Process. (ICIP)*, Sep. 2016, pp. 2246–2250, doi: 10.1109/ICIP.2016.7532758.

[14] H. Zhang, X. Liu, Z. Huang, and Y. Ji, "Single image dehazing based on fast wavelet transform with weighted image fusion," in *Proc. IEEE Int. Conf. Image Process. (ICIP)*, Oct. 2014, pp. 4542–4546, doi: 10.1109/ICIP.2014.7025921.

[15] Q. Zhu, J. Mai, and L. Shao, "A fast single image haze removal algorithm using color attenuation prior," *IEEE Trans. Image Process.*, vol. 24, no. 11, pp. 3522–3533, Nov. 2015, doi: 10.1109/TIP.2015.2446191.

[16] A. Sabir, K. Khurshid, and A. Salman, "Segmentation-based image defogging using modified dark channel prior," *EURASIP J. Image Video Process.*, vol. 2020, no. 1, pp. 1–14, Feb. 2020, doi: 10.1186/s13640-020-0493-9.

[17] R. M. Yousaf, H. A. Habib, Z. Mehmood, A. Banjar, R. Alharbey, and O. Aboulola, "Single image dehazing and edge preservation based on the dark channel probability-weighted moments," *Math. Problems Eng.*, vol. 2019, pp. 1–11, Dec. 2019, doi: 10.1155/2019/9721503.

[18] K. He, J. Sun, and X. Tang, "Single image haze removal using dark channel prior," *IEEE Trans. Pattern Anal. Mach. Intell.*, vol. 33, no. 12, pp. 2341–2353, Dec. 2011, doi: 10.1109/TPAMI.2010.168.

[19] G. Meng, Y. Wang, J. Duan, S. Xiang, and C. Pan, "Efficient image dehazing with boundary constraint and contextual regularization," in *Proc. IEEE Int. Conf. Comput. Vis.*, Dec. 2013, pp. 617–624, doi: 10.1109/ICCV.2013.82.

[20] C. O. Ancuti and C. Ancuti, "Single image dehazing by multi-scale fusion," *IEEE Trans. Image Process.*, vol. 22, no. 8, pp. 3271–3282, Aug. 2013, doi: 10.1109/TIP.2013.2262284.

[21] J. Jackson, O. Ariyo, K. Acheampong, M. Boakye, E. Frimpong, E. Ashalley, and Y. Rao, "Hybrid single image dehazing with bright channel and dark channel priors," in *Proc. 2nd Int. Conf. Image, Vis. Comput. (ICIVC)*, Jun. 2017, pp. 381–385, doi: 10.1109/ICIVC.2017.7984582.

[22] Z. Li and J. Zheng, "Single image de-hazing using globally guided image filtering," *IEEE Trans. Image Process.*, vol. 27, no. 1, pp. 442–450, Jan. 2018, doi: 10.1109/TIP.2017.2750418.

[23] Y. Liu, H. Li, and M. Wang, "Single image dehazing via large sky region segmentation and multiscale opening dark channel model," *IEEE Access*, vol. 5, pp. 8890–8903, 2017, doi: 10.1109/ACCESS.2017.2710305.

[24] S. Salazar-Colores, E. Cabal-Yepez, J. M. Ramos-Arreguin, G. Botella, L. M. Ledesma-Carrillo, and S. Ledesma, "A fast image dehazing algorithm using morphological reconstruction," *IEEE Trans. Image Process.*, vol. 28, no. 5, pp. 2357–2366, May 2019, doi: 10.1109/TIP.2018.2885490.

[25] S. Zhang and W. Bai, "Single image dehazing based on dark channel prior with different atmospheric light," in *Proc. 12th Int. Joint Conf. Comput. Vis., Imag. Comput. Graph. Theory Appl.*, 2017, pp. 224–229, doi: 10.5220/0006154702240229.

[26] W. Lu, J. Duan, Z. Qiu, Z. Pan, R. W. Liu, and L. Bai, "Implementation of high-order variational models made easy for image processing," *Math. Methods Appl. Sci.*, vol. 39, no. 14, pp. 4208–4233, Sep. 2016, doi: 10.1002/mma.3858.

[27] Q. Shu, C. Wu, Q. Zhong, and R. W. Liu, "Alternating minimization algorithm for hybrid regularized variational image dehazing," *Optik*, vol. 185, pp. 943–956, May 2019, doi: 10.1016/j.ijleo.2019.04.002.

[28] R. W. Liu, S. Xiong, and H. Wu, "A second-order variational framework for joint depth map estimation and image dehazing," in *Proc. IEEE Int. Conf. Acoust., Speech Signal Process. (ICASSP)*, Apr. 2018, pp. 1433–1437, doi: 10.1109/ICASSP.2018.8462394.

[29] Q. Shu, C. Wu, Z. Xiao, and R. W. Liu, "Variational regularized transmission refinement for image dehazing," in *Proc. IEEE Int. Conf. Image Process. (ICIP)*, Sep. 2019, pp. 2781–2785, doi: 10.1109/ICIP.2019.8803256.
[30] S. Salazar-Colores and I. Cruz-Aceves, "Single image dehazing using a multilayer perceptron," *J. Electron. Imag.*, vol. 27, no. 4, p. 1, Jul. 2018, doi: 10.1117/1.JEI.27.4.043022.
[31] K. Yuan, J. Wei, W. Lu, and N. Xiong, "Single image dehazing via NIN-DehazeNet," *IEEE Access*, vol. 7, pp. 181348–181356, 2019, doi: 10.1109/ACCESS.2019.2958607.
[32] Y. Song, J. Li, X. Wang, and X. Chen, "Single image dehazing using ranking convolutional neural network," *IEEE Trans. Multimedia*, vol. 20, no. 6, pp. 1548–1560, Jun. 2018, doi: 10.1109/TMM.2017.2771472.
[33] K. Kaul and S. Sehgal, "Single image dehazing using neural network," in *Proc. 10th Int. Conf. Cloud Comput., Data Sci. Eng. (Confluence)*, Jan. 2020, pp. 205–211, doi: 10.1109/Confluence47617.2020.9057936.
[34] F. Kou, W. Chen, C. Wen, and Z. Li, "Gradient domain guided image filtering," *IEEE Trans. Image Process.*, vol. 24, no. 11, pp. 4528–4539, Nov. 2015, doi: 10.1109/TIP.2015.2468183.
[35] M. Sulami, I. Glatzer, R. Fattal, and M. Werman, "Automatic recovery of the atmospheric light in hazy images," in *Proc. IEEE Int. Conf. Comput. Photography (ICCP)*, May 2014, pp. 1–11, doi: 10.1109/ICCPHOT.2014.6831817.
[36] R. Fattal, "Dehazing using color-lines," *ACM Trans. Graph.*, vol. 34, no. 1, pp. 1–13, Dec. 2014, doi: 10.1145/2651362.
[37] N. Hautiere, J. Tarel, D. Aubert, and E. Dumont, "Blind contrast enhancement assessment by gradient rationing at visible edges," *Image Anal. Stereology J.*, vol. 27, no. 2, pp. 87–95, 2008, doi: 10.5566/ias.v27.p87-95.
[38] X. Zhu, Y. Li, and Y. Qiao, "Fast single image dehazing through edge-guided interpolated filter," in *Proc. 14th IAPR Int. Conf. Mach. Vis. Appl. (MVA)*, May 2015, pp. 443–446, doi: 10.1109/MVA.2015.7153106.
[39] S. K. Dhara, M. Roy, D. Sen, and P. Kumar Biswas, "Color cast dependent image dehazing via adaptive airlight refinement and non-linear color balancing," *IEEE Trans. Circuits Syst. Video Technol.*, vol. 31, no. 5, pp. 2076–2081, May 2021, doi: 10.1109/TCSVT.2020.3007850.

SYED MUHAMMAD EHSAN was born in Pishin, Quetta, Pakistan, in 1995. He received the B.S. degree in electronic engineering from the Balochistan University of Information Technology, Engineering and Management Sciences (BUITEMS), Quetta, in 2017, where he is currently pursuing the master's degree.

He received funding from Space and Upper Atmosphere Research Commission, Pakistan, for a project to build low noise amplifier for satellite communication. His research interests include image denoising and de-hazing for satellite images. He was a recipient of the BUITEMS' Fee Waiver Scholarship, from 2014 to 2017.

MUHAMMAD IMRAN received the bachelor's degree from the Mehran University of Engineering and Technology, Jamshoro, the M.S. degree from NUST, Islamabad, and the Ph.D. degree from Florida State University, Tallahassee, FL, USA. He is currently working as an Assistant Professor with the Department of Electrical Engineering, Faculty of Information and Communication Technology, BUITEMS, Quetta, where he has been a Faculty Member, since 2007. He is also associated with the Control, Automotive and Robotics Laboratory (CARL), as a Co-Principal Investigator, to develop the bio-inspired robots using the cutting edge artificial intelligence technologies. He is collaborating with other institutes, working on tissue image analysis, particularly for the diagnosis of cancer. His research interests include digital signal processing and digital image processing, and ranging from theory to design to implementation. He has collaborated actively with researchers in several other disciplines of computer science, particularly on problems like image enhancements, image fusion techniques, and image matting. He worked on projects including the development of data concealing techniques for SUPARCA, Pakistan, and analysis of damages to ITS, traffic control, and roadway lighting equipment from transient surge and lightning strikes funded by the Florida Department of Transportation, USA.

ANAYAT ULLAH is currently working as an Associate Professor with the Department of Electronic Engineering, Balochistan University of Information Technology, Engineering and Management Sciences (BUITEMS), where he heads the Control, Automotive and Robotics Laboratory (CARL). He specializes in fabrication and mechanical and optical optimization of MEMS and nanoimprinted sensors. He has focused more on application of machine learning algorithms in the mathematical modeling of optical systems, such as photonic crystals. His laboratory is focus on learning-based control algorithms and data analytics using machine learning and satellite images.

ERSIN ELBASI received the M.Sc. degree in computer science from Syracuse University, and the M.Phil. and Ph.D. degrees in computer science from The Graduate Center, The City University of New York.

He is currently working with the American University of the Middle East. His research interests include multimedia security, event mining in video sequences, and medical image processing.